Radial Compression of a Non-neutral Plasma in a Non-uniform Magnetic Field of a Cusp Trap

H. Saitoh[*,†], A. Mohri[*], Y. Enomoto[*,**], Y. Kanai[*] and Y. Yamazaki[*,**]

[*]*Atomic Physics Laboratory, RIKEN, Wako 351-0198, Japan*
[†]*Graduate School of Frontier Sciences, University of Tokyo, Kashiwa 277-8561, Japan*
[**]*Graduate School of Arts and Sciences, University of Tokyo, Komaba 153-8902, Japan*

Abstract. Spectroscopic comparison of antihydrogen and hydrogen atoms is one of the best candidates for the stringent tests of the CPT symmetry, and intensive studies are being carried out by using Antiproton Decelerator at CERN. The ASACUSA collaboration has constructed a superconducting cusp trap for the formation, trapping and extraction of antihydrogen atoms, where a quadrupole magnetic field is generated by a pair of anti-Helmholtz coils with anti-parallel currents. The cusp configuration is considerably advantageous for the extraction of spin-polarized and ground-state antihydrogen beams that are ideal for the spectroscopic measurements of hyperfine structures of the ground state of antihydrogen. For the effective generation of antihydrogen atoms, it is essential to form high density and stable plasmas of antiproton and positrons. In this study, we applied a rotating electric field to an electron plasma in the inhomogeneous cusp magnetic field, and demonstrated the effective radial compression of a non-neutral plasma in a broad frequency range. The compression rate depended on the rotating frequency and had a broad peak extending on both sides of a longitudinal (1,0) mode frequency, which was the only observed characteristic frequency. The similar procedure can in principle be applied to positron and antiproton plasmas, and the results are one of necessary steps toward antihydrogen experiments in the cusp trap.

Keywords: non-neutral plasma, pure electron plasma, cusp magnetic field, antihydrogen synthesis
PACS: 37.10.-x, 52.27.Jt, 36.10.-k, 52.27.Aj

INTRODUCTION

Compression techniques of charged particles have a wide range of scientific applications in the fields of non-neutral plasma, atomic, and particle physics. Recently, experiments on antihydrogen synthesis are being carried out intensively by using the Antiproton Decelerator (AD) [1] at CERN. Spectroscopic comparison of antihydrogen atoms with hydrogen ones provides one of the stringent tests of the CPT symmetry, and so far two groups have succeeded the production of cold antihydrogen atoms [2, 3]. For efficient production of antihydrogen atoms in these experiments, a method to form high density antiproton and positron plasmas is one of the essential issues.

In the antihydrogen experiments carried out at CERN, 5.3 MeV antiprotons from the AD were decelerated, trapped, and mixed with positron plasmas to form antihydrogen atoms via recombination processes in uniform magnetic fields of "nested" Penning traps. In a trap with a uniform magnetic field, however, the generated neutral atoms feel no attracting or repulsive forces, and therefore it is not straightforward to manipulate antihydrogen atoms for further spectroscopic studies. For future experiments on high-precision laser or microwave spectroscopy of antihydrogen aiming for the CPT symmetry test, it is required that the generated antihydrogen atoms in high Rydberg states are trapped for

a time long enough for cascade down to their ground state [11, 12, 13]. Antihydrogen atoms with a magnetic moment μ undergo $-\mu\nabla|\mathbf{B}|$ force in an inhomogeneous magnetic field $\mathbf{B}$, and thus cold antihydrogen atoms in the low-field seeking states can in principle be confined in minimum-B magnetic field configurations [14, 15].

Several approaches are being made to introduce a magnetic gradient on a trap geometry and to simultaneously confine both neutral hydrogen atoms and non-neutral plasmas. In the standard Ioffe-Pritchard trap [16], the quadrupole field of Ioffe bars breaks the axial symmetry of a magnetic configuration, which may lead to instability or rapid losses of non-neutral plasmas [17]. A new experiment was proposed for antihydrogen spectroscopy by using a trap with octupole magnetic field for reducing the field asymmetry and resultant perturbations, and both confinement and compression of antimatter plasmas were successfully demonstrated without significant diffusive loss [18].

In the ASACUSA collaboration, the use of a cusp magnetic field configuration (an axisymmetric magnetic quadrupole) has been proposed for the scheme to synthesize and trap cold antihydrogen atoms [19, 20, 21, 22, 12]. When antiproton and positron clouds are mixed near the magnetic null point of the cusp trap, cold antihydrogen atoms are synthesized and extracted as ultra-slow spin-polarized beams. In this study, we have carried out experiments on electron plasmas in a spindle cusp region in order to understand the basic properties of non-neutral plasmas in the cusp field. We applied a rotating wall technique to the cusp non-neutral plasma and found a way to make an effective radial compression. Although the application of the RF field of the rotating wall heated up the plasma, the synchrotron radiation in the strong cusp magnetic field quickly cooled the plasma, and as a result a cold and high density plasma was successfully formed [21].

EXPERIMENTAL SETUP

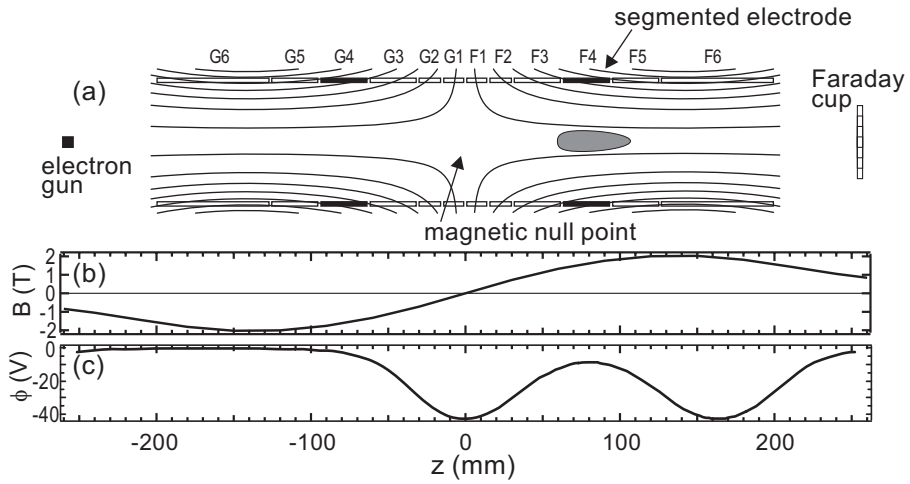

FIGURE 1. (a) Schematic view of the trap electrodes and typical (b) magnetic and (c) electrostatic potential profiles on the device axis $r = 0$.

Schematic view of the trap and field profiles of the superconducting cusp device [21] is shown in Fig. 1. The trap configuration is generated by the combination of a cusp

magnetic field, expressed by a vector potential $A_\theta(r,z) = (B_0/L)rz$ in the cylindrical coordinates (r,θ,z), and an electrostatic potential. The "throat" of the field lines is located at $z = \pm 150$ mm, where the maximum field strength on the device axis is 2.0 T at the coil current of 60 A. In the confinement region of the trap, the typical field strength in this experiment was 1.6 T at $z = \pm 80$ mm. The variation of the field strength at $z = 40$ - 120 mm was 55%. The trap consists of twelve cylindrical electrodes of the inner diameter of 80 mm. In the trap region, a harmonic electrostatic potential $\phi_V(r,z) = -\phi_0 \left[(z-L)^2 - r^2\right]/L^2$ was applied. The trap system was evacuated to the base pressure of 2×10^{-7} Pa. As shown in Fig. 1 (c), the potential well for electron trap was located near $z = L = +80$ mm. Here ϕ_0/L^2 was set in the range from 3.6×10^3 to 1.1×10^4 V/m^2 in the experiment. In the most often used case, $\phi_0/L^2 = 9.0 \times 10^3$ V/m^2 and the depth of the potential well was 30 V. The longitudinal bounce motion of an electron in the potential well is approximated as a harmonic oscillation of frequency $f_b = \sqrt{e\phi_0/2\pi^2 m_e L^2} = 9.0$ MHz. In Fig. 1 (a), F4 is a segmented electrode that was used for applying an azimuthally rotating $m = 1$ electric field to the plasma. Sinusoidal RF on the four electrode segments had phase differences of $\pi/2$ in the direction parallel or opposite to the $\mathbf{E} \times \mathbf{B}$ plasma rotation and f_{RW} was < 15 MHz.

Electrons were injected by an electron gun as a train of pulsed beams. In the injection phase, the potential wall on the electron gun side was lowered synchronously to the arrival of each beam pulse and thereby electrons were trapped inside the potential well. Electrons were dumped on a Faraday cup located at the downstream side of the trap (see Fig. 1 (a)). The Faraday cup is coaxially segmented into eight with the radial pitch of 4 mm and the total diameter is 60 mm, which allows to monitor the line-integrated density n_l (integration of density along magnetic field lines) of the electron plasma. We also measured the parallel electron temperature by shallowing the potential wall and analyzing the energy profiles of escaping electrons [23].

EXPERIMENTAL RESULTS AND DISCUSSION

Excitation of characteristic modes

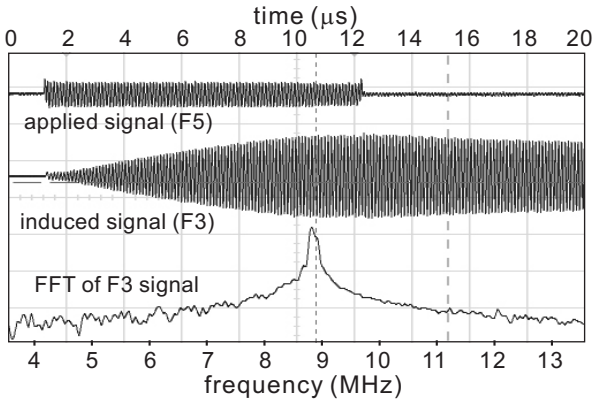

FIGURE 2. Response of plasma on external fluctuations. Applied RF frequency was 8.9 MHz, in resonance with the characteristic plasma frequency f_z.

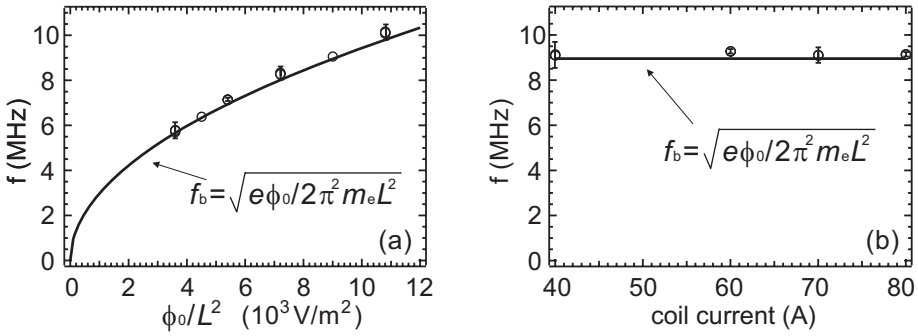

FIGURE 3. Observed resonant frequencies f_z as functions of (a) gradient of the external electrostatic potential well, represented by ϕ_0/L^2, and (b) cusp magnetic field strength.

Figure 2 shows the excitation of plasma oscillation modes. An external RF was applied in the longitudinal direction of the device by using F5. When the applied RF resonated with a mode of frequency f_z, the amplitude of the excited plasma oscillation grew almost linearly, as shown in Fig. 2. This mode was also excited in an off-resonant condition if the RF input was large enough. By sweeping the frequency of sinusoidal wave on F5 from 10 kHz to 30 MHz, we found only one resonant mode corresponding to the center of mass oscillation of an electron plasma: $f_z = f_b$. Figure 3 shows the frequencies of the observed oscillation mode f_z as functions of ϕ_0 and the coil current being proportional to the magnetic field strength B. The mode frequency had a dependence of $f_z \propto E^{1/2}B^0$, where E is the external electric field strength. The solid curve f_b in Fig. 3 well reproduces the observed mode frequencies. Although the electron temperature varied during the confinement cycle, as discussed later, the observed frequency stayed constant [24].

Radial compression of cusp plasmas by using a rotating wall

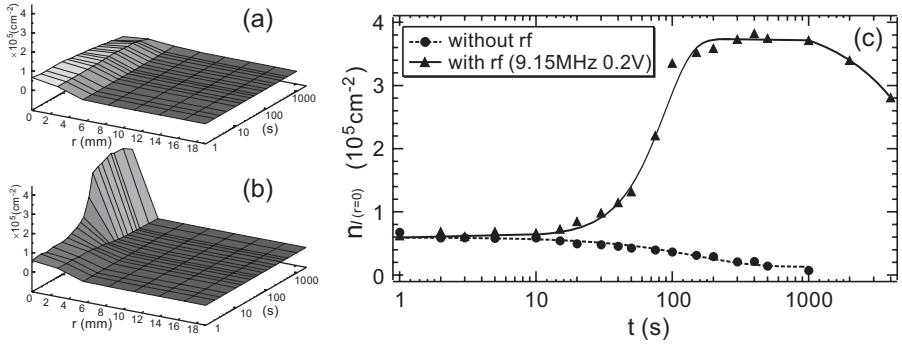

FIGURE 4. Temporal evolution of the line-integrated density profiles of a plasma (a) with and (b) without the rotating wall, and (c) n_l: line-integrated density at $r = 0$. The solid and dotted lines are to guide the eyes only.

Temporal evolutions of n_l profiles were measured by the Faraday cup as displayed in Fig. 4. When the rotating wall was not applied (Fig. 4 (a), circles in (c)), the plasma radially expanded, and after $t \sim 400$ s, the total electron number decreased with a $1/e$

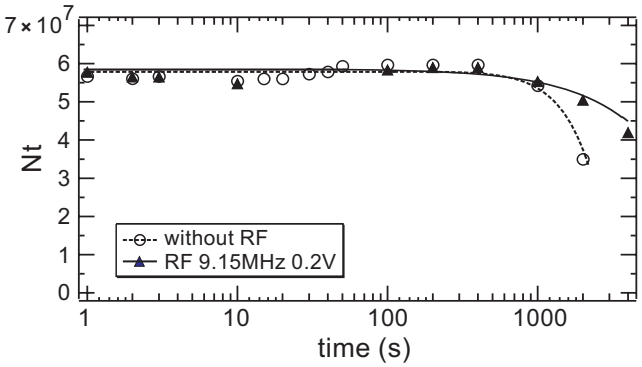

FIGURE 5. Temporal evolutions of total trapped charge with and without application of rotating RF.

time constant of 3000 s as shown in the circles in Fig. 5. The line-integrated density at $r = 0$ was $n_{l(r=0)} = 6.7 \times 10^4$ cm^{-2} at $t = 1$ s, and decreased to $n_{l(r=0)} = 7.2 \times 10^3$ cm^{-2} at $t = 1000$ s with a time constant of τ_E = 150 s.

In contrast, by applying the rotating wall, effective compression was observed as shown in Fig. 4 (b). The rotating wall was applied in the direction of the $\mathbf{E} \times \mathbf{B}$ rotation of the plasma at the frequency of $f_{RW} = 9.15$ MHz, which was 0.25 MHz higher than f_z. The amplitude of the applied RF was $V_{RW} = 0.2$ V. The solid triangles with the fitting curve in Fig. 4 (c) show that n_l increased and it saturated at $t \sim 400$ s, where $n_{l(r=0)} = 3.8 \times 10^5$ cm^{-2}. After the application of the rotating wall for 400 s, 74 % of the initial electrons were radially compressed into the central region ($r < 1.4$ mm). The total number and $n_{l(r=0)}$ were both unchanged for 1000 s after reaching the peaky density profile (Fig. 5).

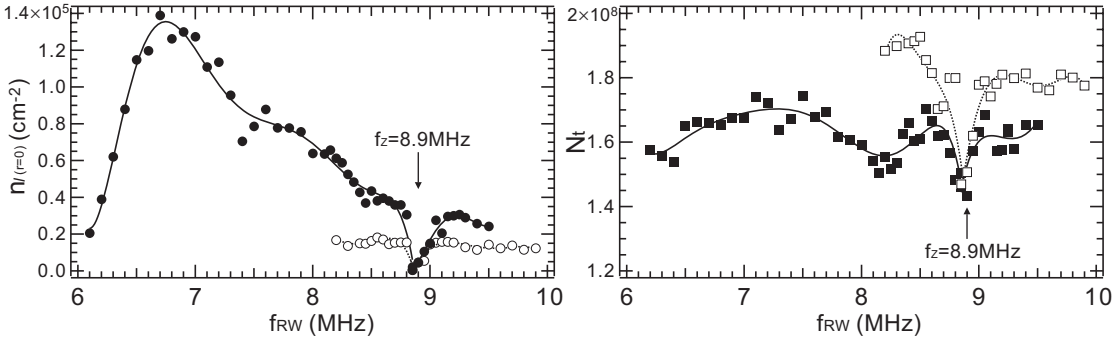

FIGURE 6. Total electron number N_t and line-integrated density on the device axis $n_{l(r=0)}$ at $t = 20$ s as a function of applied rotating wall frequency. Directions of the applied rotating wall were equal to (solid circles and solid squares) and opposite to (open circles and open squares) the $\mathbf{E} \times \mathbf{B}$ plasma rotation.

In Fig. 6, the central line-integrated density $n_{l(r=0)}$ and the total electron number N_t were measured after the application of the rotating wall for 20 s. When the rotating wall was not applied, $n_{l(r=0)} = 2.1 \times 10^4$ cm^{-2}. When the rotating wall was applied in the $\mathbf{E} \times \mathbf{B}$ rotation direction, radial compression was observed in a broad f_{RW} range from approximately 6 MHz to 9.5 MHz except for frequencies from 8.85 MHz to 9.0 MHz. When f_{RW} was close to the observed longitudinal resonance mode frequency of $f_z = 8.9$ MHz, both the numbers of electrons in the central region and the total

electrons decreased quickly regardless of the rotation direction.

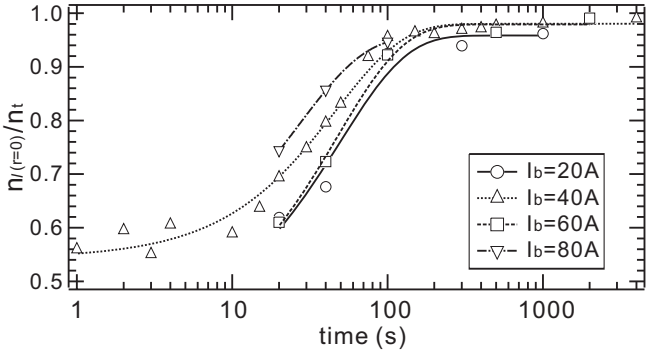

FIGURE 7. Central plasma density normalized by the average density for four different coil currents. Frequency of the applied rotating wall RF was 9.15 MHz

Figure 7 shows the temporal evolutions of the central plasma density (normalized by the average density) for four different coil currents. The rotating wall RF with an amplitude of 0.6 V was applied for 20 s. The compression effects were similarly observed in the all applied coil current values, and there was no strong dependence on B. The typical time constant of the compression was of the order of ~ 100 s.

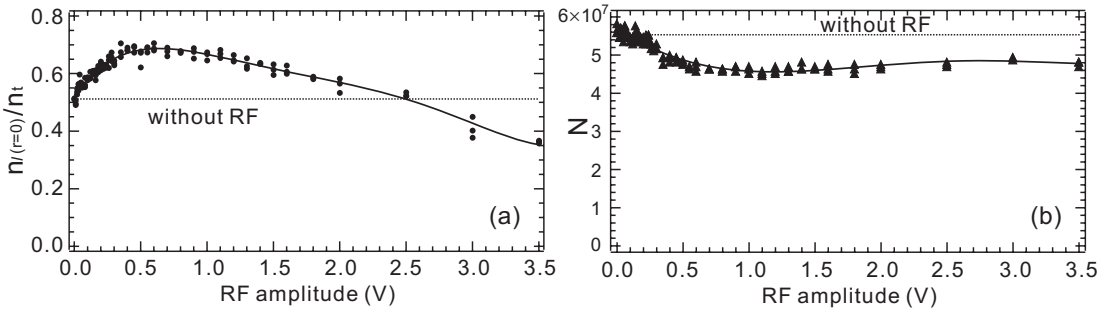

FIGURE 8. (a) Compression effect and (b) total electron number for different rotating RF amplitude. Rotating wall RF of 9.15 MHz was applied for 20 s.

Figure 8 shows the central plasma density for different RF amplitude V_{RF} of the rotating wall. When the RF was not applied, $n_{l(\mathrm{r}=0)}/n_{\mathrm{t}} = 0.51$ after 20 s of confinement. The compression efficiency had a broad peak around $V_{\mathrm{RF}} = 0.6$ V, and as V_{RF} was further increased, effective compression was not observed above $V_{\mathrm{RF}} = 2.5$ V. As described later, application of the rotating wall heats the plasma, but cyclotron radiation cooling prevents the increase of the temperature.

Electron temperature

As shown in Fig. 9, temporal evolutions of the electron temperature parallel to **B**, $T_{\mathrm{e}\|}$, was measured by using the energy distribution of electrons leaked to the Faraday cup. In the initial phase of confinement at $t = 0.2$ s, $T_{\mathrm{e}\|} = 5.7$ eV. When the rotating wall field was not applied, it cooled quickly and reached 0.4 eV in $t = 10$ s and after then

stayed almost constant. Such a steady state is also another side-evidence on the existence of a rigid-rotor equilibrium of a non-neutral plasma in the spindle cusp configuration. The observed $1/e$ cooling time of $T_{e\|}$ was 2.5 s, which is comparable to the typical cooling time caused by the synchrotron radiation in a magnetic field given by the Larmor formula for the typical field strength $B = 1.6$ T: $\tau_D \sim 3\pi\varepsilon_0 m_e c^3/e^2\omega_{ec}^2 \sim 1.0$ s. Although the variation of field strength was small, quicker cooling was observed for stronger B as shown in Fig. 9 (b). The parallel electron temperature did not decrease lower than 0.4 eV, which could be due to the effects of the warm bore and external noise. Further study will be carried out in the near future using a cryogenic cusp trap.

The closed triangles in Fig. 9 (a) show the temperature evolution when the rotating wall was turned on, which revealed that it reached an equilibrium of $T_{e\|} = 1.7$ eV, four times higher than that without the rotating wall. When the RF was turned off, $T_{e\|}$ dropped to the same temperature 0.4 eV as in the case of no RF application, and this cooling rate was comparable to τ_D as shown in Fig. 9 (b). The time scale of the radial expansion of the compressed plasma $\tau_E \sim 150$ s is much longer than τ_D, and the rotating wall can significantly compress the plasma practically keeping the plasma temperature unchanged.

In future experiments, a positron plasma in one side of a spindle cusp will be transported to the opposite side in order to induce recombinations with antiprotons to form antihydrogen atoms. In this process, particles located near the center axis of the device are primarily transferred through the magnetic null point, and the plasma may take unstable hollow structures. The rotating wall can be utilized for the stable transfer of positrons by the radial compression that compensate the decrease of particles on the device axis.

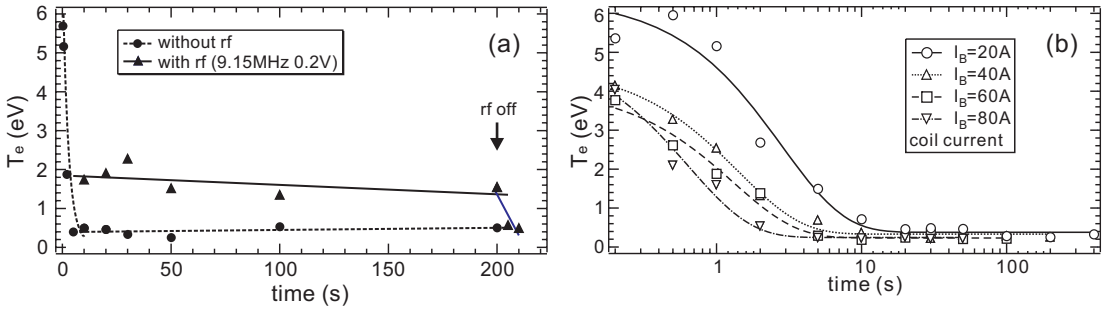

FIGURE 9. Temporal evolutions of $T_{e\|}$ (a) when the rotating wall was applied from $t = 0$ to 200 s (triangles) and not applied (circles) and (b) in the variation of field strength without the application of rotating wall.

CONCLUSION

To summarize, we have demonstrated that a single-component plasma in the inhomogeneous cusp magnetic field can be effectively compressed by using the rotating wall technique as in the case of a plasma in a uniform magnetic field. The compression was observed with a broad frequency range of a rotating wall in the $\mathbf{E} \times \mathbf{B}$ velocity direction except for frequencies close to the longitudinal resonance frequency of the plasma, which is the only observed mode of a spindle cusp electron plasma. The compression

and cooling of an electron plasma were simultaneously realized. Although the present experiment was carried out using an electron plasma, the same procedure can in principle be applied to a positron plasma, which is particularly important for the formation and extraction of antihydrogen atoms.

ACKNOWLEDGMENTS

This work was funded by Special Research Projects for Basic Science of RIKEN. The work of H. S. was supported in part by the Special Postdoctoral Researchers Program of RIKEN.

REFERENCES

1. S. Maury, Hyperfine Interact., **109**, 43 (1997).
2. M. Amoretti *et al.*, Nature **419**, 456 (2002).
3. G. Gabrielse *et al.*, Phys. Rev. Lett. **89**, 213401 (2002).
4. X.-P. Huang, F. Anderegg, E. M. Hollmann, C. F. Driscoll, and T. M. O'Neil, Phys. Rev. Lett. **78**, 875 (1997).
5. X.-P. Huang, J. J. Bollinger, T. B. Mitchell, and W. M. Itano, Phys. Rev. Lett. **80**, 73 (1998).
6. F. Anderegg, E. M. Hollmann, C. F. Driscoll, Phys. Rev. Lett. **81**, 4875 (1998).
7. E. M. Hollmann, F. Anderegg, C. F. Driscoll, Phys. Plasmas **7**, 2776 (2000).
8. Y. Soga, Y. Kiwamoto, and N. Hashizume, Phys. Plasmas **13**, 052105 (2006).
9. J. R. Danielson and C. M. Surko, Phys. Rev. Lett. **94**, 035001 (2005); J. R. Danielson and C. M. Surko, Phys. Plasmas **13** 055706 (2006).
10. R. G. Greaves and C. M. Surko, Phys. Rev. Lett. **85** 1883 (2000); R. G. Greaves and C. M. Surko, Phys. Plasmas **8**, 1879 (2001).
11. Y. Yamazaki, Physica Scripta **T110**, 286 (2004).
12. T. Pohl, H. R. Sadeghpour, Y. Nagata, and Y. Yamazaki, Phys. Rev. Lett. **97**, 213001 (2006).
13. W. Bertsche *et al.*, Nucl. Instrum. Methods Phys. Res., Sect. A **521**, 746 (2006).
14. T. M. Squires, P. Yesley, and G. Gabrielse, Phys. Rev. Lett. **86**, 5266 (2001).
15. D. H. Dubin, Phys. Plasmas **8** 4331 (2001).
16. D. E. Pritchard, Phys. Rev. Lett. **51**, 1336 (1983).
17. E. P. Gilson and J. Fajans, Phys. Rev. Lett. **90**, 015001 (2003).
18. G. Andresen *et al.*, Phys. Rev. Lett. **98**, 023402 (2007).
19. A. Mohri *et al.*, Jpn. J. Appl. Phys. **37**, **L**1553 (1998).
20. A. Mohri and Y. Yamazaki, EuroPhys. Lett. **63**, 207 (2003).
21. A. Mohri *et al.*, in *Physics with Ultra Slow Antiproton Beams* (AIP Conf. Procs. **793**), 147 (2005); A. Mohri *et al.*, in Procs. EPS Conf. Plasma Phys P-4.067 (2006); H. Saitoh *et al.*, Phys. Rev. A **77**, 051403 (2008).
22. N. Kuroda *et al.*, Phys. Rev. Lett. **94**, 023401 (2005); N. Kuroda *et al.*, Phys. Rev. Lett. **100**, 203402 (2008).
23. B. R. Beck, J. Fajans, and J. H. Malmberg, Phys. Rev. Lett. **68**, 317 (1992).
24. H. Higaki and A. Mohri, Jpn. J. Appl. Phys. **36**, 5300 (1997).